Wavefield separation using the f–ξ domain for vertical seismic profiling data

Baotong Liu[1,*], *Qiyuan* Liu[2], *Yingshuang* Jiang[1], *Donglin* Liu[1], and *Xuefu* Kang[1]

[1]School of Electronic Information and Electrical Engineering, Tianshui Normal University, Tianshui 741001, China
[2]School of Mathematics, Sichuan University, Chengdu 610064, China

Abstract. Wavefield separation is an essential and critical step in data processing of vertical seismic profiles (VSPs). The τ–p transform is one of the effective approaches for separating the VSP wavefield. To further improve the efficiency of the τ–p transform, we developed an f–ξ domain τ–p transform based on the high-resolution Radon transform. The introduction of a new variable ξ removes the frequency dependence of the transform operator. As a result, the transform operator needs to be computed only once for all frequency components, which significantly improves the computational efficiency without decreasing accuracy. Furthermore, because the events of upgoing and downgoing waves are distributed in the vicinity of straight lines with different slopes through the origin in the f–ξ domain, we can easily define a filter to separate the upgoing and downgoing waves. Model tests showed that the wavefields are well separated and that the new method is a factor of ~3 faster than its counterpart in the τ–p domain. The field data example further demonstrates the effectiveness and feasibility of the approach.

1 Introduction

Seismic exploration has been successfully applied in the petroleum industry for a long time. Vertical seismic profiles (VSP) have been viewed as an attractive tool, both for exploration purposes and for time-lapse monitoring of reservoirs [1]. However, interference between the downgoing and upgoing waves hinders further processing such as imaging or amplitude versus offset analysis. Both the upgoing and downgoing waves are useful but need to be separated before proceeding with processing and interpretation [2]. Therefore, development of wavefield separation technologies has attracted the attention of prospecting geophysicists. Many methods have been developed for separating VSP wavefields over the past five decades. Among them, median filtering, f–k filtering, singular value decomposition, and τ–p filtering are in common use.

The τ–p transform has found wide application in seismic data processing, such as for ground-roll attenuation, migration, primary and multiple separation, offset interpolation, and wavefield separation [3-5, 7]. In VSP sections, the upgoing and downgoing events have opposite apparent slowness (inverse apparent velocity). After application of the τ–p

* Corresponding author: liubt163@163.com

transform, the upgoing and downgoing energy signals are separated and mapped into different quadrants of the τ–p plane. Therefore, the upgoing and downgoing waves become separable. However, the numerical computation of the τ–p transform suffers from the smearing problem (in which the energy of seismic events spread out and cross-hatch the τ–p spectrum), which is caused by the limited size of the spatial aperture of a seismic section [6]. Performing the τ–p transform to obtain resolution beyond this limit is an ill-posed inverse problem [3-5]. Many different ways have been investigated for obtaining the τ–p transform, but the most commonly used is that of inversion [3, 7].

The τ–p transform can be implemented in the frequency domain via the damped least-squares algorithm [6], known as the standard inversion. Owing to the Toeplitz structure of the transform operator, the standard inversion can be solved by means of the Levinson recursion algorithm; this provides a very efficient approach to compute the τ–p transform. To further improve the resolution of the model space, several methods for constrained inversion have been developed [3, 4]. Sacchi and Ulrych proposed an algorithm that forces sparseness in the model space using diagonal weighting matrices in the least-squares system [7]; this is known as the high-resolution Radon transform. The method performs well and leads to a good event focus, but it entails quite high computational cost.

In this study, we developed a modified τ–p transform on the basis of the high-resolution Radon transform. In the proposed approach, we introduce a new variable ξ, which makes the transform operator independent of frequency. Consequently, transform operators need to be computed only once for all frequency components, which significantly improves the computational efficiency without decreasing accuracy. Applying this approach on VSP data leads to faster separation of upgoing and downgoing waves compared to previous implementation of the high-resolution Radon transform. In the following sections, we first present the algorithm details of this method and then apply the method to synthetic data to show the effectiveness of wavefield separation. Finally, a field data processing test verifies the practicality of the approach.

2 Algorithm design

The finite discrete form of inverse *τ–p* transform is as follows [2, 6]:

$$d(t,z_k)=\sum_{j=1}^{Np} m(t-p_j z_k,p_j), \qquad k=1,2,\cdots,Nz, \tag{1}$$

where $d(t,z_k)$ is vertical seismic data, $m(\tau,p_j)$ is the *τ–p* transform of $d(t,z_k)$, Np denotes the number of slowness p, and Nz is the number of seismic traces. Computationally, the problem becomes more efficient and manageable by transforming the time variable to the frequency domain. The Fourier transform of Eq. 1 is given as [3, 6, 7]

$$D(f,z_k)=\sum_{j=1}^{Np} M(f,p_j)\mathrm{e}^{-\mathrm{i}2\pi f p_j z_k}. \tag{2}$$

Equation 2 can be written in matrix form as

$$\boldsymbol{D}(f)=\boldsymbol{G}(f)\boldsymbol{M}(f), \tag{3}$$

where $\boldsymbol{D}$ and $\boldsymbol{M}$ are vectors of lengths Nz and Np, respectively. The elements of matrix $\boldsymbol{G}$ are given by

$$G_{kj}(f) = \mathrm{e}^{-\mathrm{i}2\pi f p_j z_k}, \quad k = 1,2,\cdots,Nz, \quad j = 1,2,\cdots,Np. \tag{4}$$

Sacchi and Ulrych proposed a constrained inversion solution of Eq. 3, known as the high-resolution Radon transform (HRT) [7], which is expressed as

$$\hat{\boldsymbol{M}}(f) = \left[\boldsymbol{G}^{\mathrm{H}}(f)\boldsymbol{G}(f) + \varepsilon^2 diag\left(\frac{1}{1+\frac{m_i^2}{b^2}} \right) \right]^{-1} \boldsymbol{G}^{\mathrm{H}}(f)\boldsymbol{D}(f), \tag{5}$$

where H denotes the complex conjugate transpose, *diag* defines a diagonal operator, and ε and b are two constants chosen a priori.

Equation 5 requires computing the transform for each frequency component in the signal bandwidth. The complex operator $\boldsymbol{G}(f)$ is frequency dependent, leading to a different matrix for each frequency component. Therefore, in computations of Eq. 5, $\boldsymbol{G}(f)$, $\boldsymbol{G}^{\mathrm{H}}(f)$, and $\boldsymbol{G}^{\mathrm{H}}(f)\boldsymbol{G}(f)$ have to be computed for each spectral component. Applying Eq. 5 in the separation of the VSP wavefield is expensive, degrading processing efficiency. To remove the frequency dependence in the transform operator $\boldsymbol{G}(f)$, we introduce a new variable $\xi = pf$ with units of m^{-1}. As a result, Eqs. 4 and 5 become

$$G_{kj}(\xi) = \mathrm{e}^{-\mathrm{i}2\pi\xi_j z_k}, \qquad k = 1,\cdots,Nz, \qquad j = 1,\cdots,N\xi, \tag{6}$$

$$\hat{\boldsymbol{M}}(f) = \left[\boldsymbol{G}^{\mathrm{H}}(\xi)\boldsymbol{G}(\xi) + \varepsilon^2 diag\left(\frac{1}{1+\frac{m_i^2}{b^2}} \right) \right]^{-1} \boldsymbol{G}^{\mathrm{H}}(\xi)\boldsymbol{D}(f). \tag{7}$$

The matrix $\boldsymbol{G}(\xi)$ is frequency independent. Hence, in computations of Eq. 7, $\boldsymbol{G}(\xi)$, $\boldsymbol{G}^{\mathrm{H}}(\xi)$, and $\boldsymbol{G}^{\mathrm{H}}(\xi)\boldsymbol{G}(\xi)$ need to be computed only once for all frequency components. Applying Eq. 7 in the separation of VSP wavefields reduces computational cost, improving processing efficiency.

In performing the τ–p transform, to avoid aliasing, parameters $p_{\min}$, $p_{\max}$, and Δp must meet the following conditions [2, 6]:

$$\Delta p < \frac{1}{f(z_{\max} - z_{\min})}, \qquad |p_{\max}| \le \frac{1}{2f\Delta z}, \tag{8}$$

where Δz is the depth spacing and $z_{\min}$ and $z_{\max}$ denote the maximum and minimum depths in the VSP data, respectively. Therefore, in the presented method, the following conditions must be satisfied:

$$\Delta\xi = f\Delta p < \frac{1}{z_{\max} - z_{\min}}, \qquad \left|\xi_{\max}\right| = \left|fp_{\max}\right| \le \frac{1}{2\Delta z}. \tag{9}$$

In a VSP section, the upgoing and downgoing waves have opposite apparent slowness. By applying Eq. 7 to the VSP data, the upgoing and downgoing events are mapped into different quadrants of the *f*–ξ plane; for upgoing events, $\xi < 0$, while for downgoing events, $\xi > 0$. We design the following simple filters:

$$\mathrm{FTR}^{\mathrm{u}}(f,\xi) = \begin{cases} 1, & \xi \le 0, \\ 0, & \xi > 0, \end{cases} \tag{10}$$

$$\mathrm{FTR}^{\mathrm{d}}(f,\xi) = \begin{cases} 0, & \xi \le 0, \\ 1, & \xi > 0. \end{cases} \tag{11}$$

The separated upgoing waves are given as follows:

$$\hat{\boldsymbol{M}}^{\mathrm{u}}(f) = \mathrm{FTR}^{\mathrm{u}}(f,\xi)\hat{\boldsymbol{M}}(f), \tag{12}$$

and the downgoing waves are

$$\hat{\boldsymbol{M}}^{\mathrm{d}}(f) = \mathrm{FTR}^{\mathrm{d}}(f,\xi)\hat{\boldsymbol{M}}(f). \tag{13}$$

3 Experiments with synthetic data

To verify the feasibility of the presented algorithm for wavefield separation, we applied it to two synthetic datasets. Using the staggered grid finite-difference scheme with fourth-order accuracy in time and tenth-order accuracy in space, we calculated two synthetic VSP sections and separated the upgoing and downgoing waves. The experiments were performed on a computer with an Intel® Core i7-4790 CPU operating at 3.6 GHz, having 8GB of RAM, and running Visual Fortran 4.0.

The first synthetic example is a two-layer model. Figure 1(a) shows the synthetic VSP seismograms; these consist of 70 traces with 316 samples per trace. The trace interval was 5 m. The sampling interval was 0.00025 s. The peak frequency of the Ricker wavelet was 90 Hz. Figures 1(b)–1(d) depict the τ–p spectrum (Δp = 0.0000004, $\left|p_{\max}\right|$=0.00018) and the separated upgoing and downgoing waves in the τ–p domain. Figures 1(e)–1(g) depict the *f*–ξ spectrum ($\Delta\xi$ =0.0002, $\left|\xi_{\max}\right|$=0.1) and the separated upgoing and downgoing waves in the *f*–ξ domain. The computation time for calculating the τ–p spectrum was 52 s, and that for calculating the *f*–ξ spectrum was 13 s.

The second synthetic section is a six-layer model. The depth of the source was set to 30 m, and the offset was 6 m. A zero-phase Ricker wavelet with a central frequency of 120 Hz was used to generate synthetic records. Receivers were located at depths of 135 to 590 m. The resulting synthetic VSP section is shown in Fig. 2(a). The dataset consisted of 92 traces with 350 samples per trace. The trace and sampling intervals were 5 m and 0.001 s, respectively.

When Δp = 0.000002 and p ranged from −0.0005 to +0.00044, the τ–p spectrum obtained from Eq. 5 is given in Fig. 2(b); the calculations took 85 s. The upgoing waves are mapped into the left half of the plane (p <0), and downgoing waves are mapped into the right half of the plane (p >0). The part of the τ–p plane with p >0 (or p <0) was zeroed, and the inverse transform left upgoing (or downgoing) waves as the output. Figures 2(c) and 2(d) show the downgoing and upgoing waves, respectively. In Fig. 2(a), the minimum depth $z_{\min}$ = 135 m, the maximum depth $z_{\max}$ = 590 m, and the depth interval Δz = 5 m. From Eq. 9 we obtained the bounds $\Delta\xi < 0.0022$ m^{-1} and $|\xi_{\max}| \le 0.1$ m^{-1}. We took $\Delta\xi$ = 0.0008 m^{-1} and $|\xi_{\max}|$ = 0.1 m^{-1}, thus $N\xi = 251$. The f–ξ spectrum obtained from Eq. 7 is shown in Fig. 3(a), the calculations took only 21 s. Compared to the result obtained from using Eq. 5, the computational cost is reduced significantly. The upgoing waves are mapped into the left half of the plane (ξ <0), and downgoing waves are mapped into the right half of the plane (ξ >0). The separation of upgoing and downgoing waves can be achieved via Eqs. 12 and 13. Figures 3(b) and 3(c) show the downgoing and upgoing waves, respectively.

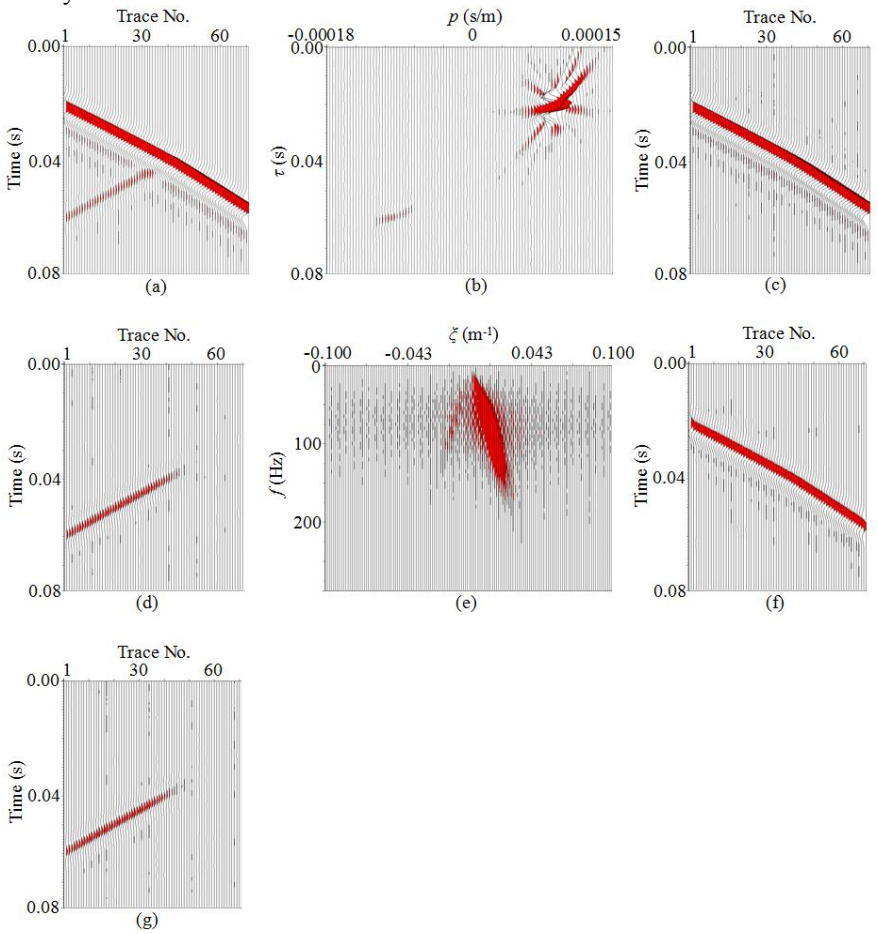

Fig. 1. Comparison of the results obtained based on the new method and the τ–p method. (a) Synthetic VSP seismograms for a two-layer model. (b) τ–p spectrum. (c) Downgoing waves separated from the τ–p spectrum. (d) Upgoing waves separated from the τ–p spectrum. (e) f–ξ spectrum. (f)

Downgoing waves separated from the f–ξ spectrum. (g) Upgoing waves separated from the f–ξ spectrum.

4 Real data example

The proposed method was tested on real VSP data acquired from an oil well in southwestern China. The depth range of receiving points was 1000–2050 m, the total number of traces used was 211, and the trace interval was 5 m. The recording length was 3 s, with a sampling interval of 0.001 s. Figure 4(a) shows the input data. Because geophones were placed in the downhole, the reflected energy is free from the weathering layer, leading to reflection waves with high resolution. The downgoing wave components demonstrate very clearly their dominance. In addition to P waves, there are the P-SV converted waves in

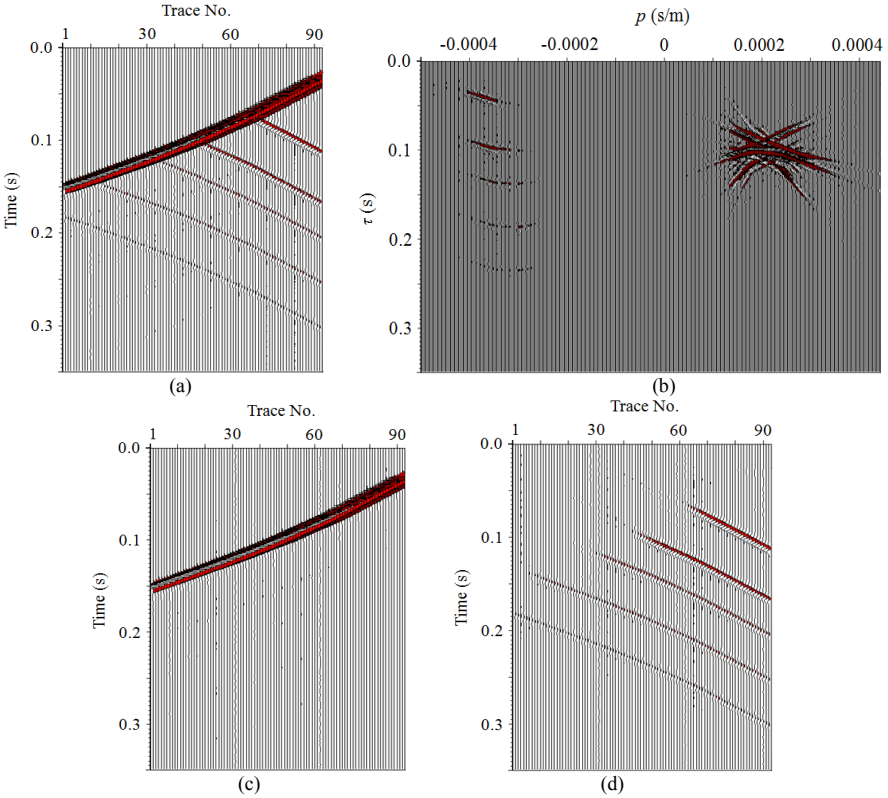

Fig. 2. Separation test in the τ–p domain. (a) Synthetic VSP section generated by using the staggered grid finite-difference scheme. (b) τ–p spectrum obtained from Eq. 8. Upgoing energy lies in the negative half of the plane ($p < 0$), and downgoing energy lies in the positive half of the plane ($p > 0$). (c) Separated downgoing waves via the τ–p spectrum. (d) Separated upgoing waves via the τ–p spectrum.

The downgoing waves. Wavefield separation must be done before the corridor stack. We separated the upgoing and downgoing waves by using the method presented in this study. Considering $z_{\min}$ = 1000 m, $z_{\max}$ = 2050 m, and a depth interval Δz = 5 m, we calculated $\Delta\xi < 0.00095$ m^{-1}, with $|\xi_{\max}| \le 0.1$ m^{-1}. In this processing, we took $\Delta\xi$ = 0.0004 m^{-1} and $|\xi_{\max}|$ = 0.1 m^{-1}. Consequently, $N\xi$ = 501. The input data were transformed into the f–ξ domain. Figure 4(b) depicts the f–ξ spectrum. The direct P waves,

converted S waves, and reflection waves map to distinct areas (marked as I, II, and III) of the f–ξ plane. Each area appears in the vicinity of a line with specific slope. We chose the filtering operator according to Eq. 10 for upgoing wave extraction and then we converted it back to the depth–time domain. Figure 4(c) shows the upgoing waves after using the presented method to remove the downgoing waves. Furthermore, after both areas II and III were zeroed, the inverse transformation left the direct P waves as the output. We can also extract the S waves by zeroing both areas I and III. Figures 4(d) and 4(e), respectively, show the separated direct P and S waves. In Figs. 4(c)–4(e), the background noise before the first break P arrival has been removed.

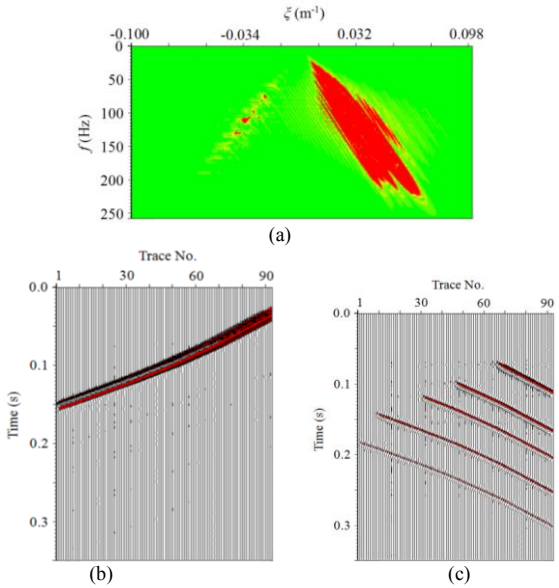

Fig. 3. Separation test in the f–ξ domain. (a) f–ξ spectrum obtained from Eq. 7. Upgoing energy lies in the negative half of the plane ($\xi < 0$), and downgoing energy lies in the positive half of the plane ($\xi > 0$). (b) Separated downgoing waves via the f–ξ spectrum. (d) Separated upgoing waves via the f–ξ spectrum.

5 Conclusions

We presented the f–ξ domain Radon transform and implemented wavefield separation in the proposed f–ξ domain. The advantages of the presented method are as follows:

1. The introduction of a new variable ξ removes the frequency dependence of the transform operator.

2. Transform operators need to be computed only once for all frequency components, which reduces computational cost significantly. The calculation cost of the proposed method is only 25% of that of the conventional high-resolution τ–p transform, with no degradation of accuracy.

3. Applying the presented algorithm to VSP data processing achieves rapid wavefield separation.

4. Model tests show that the fidelity of separated upgoing reflection waves is slightly higher than that of the conventional high-resolution τ–p transform.

The research work was supported by the National Natural Science Foundation of China (grant no. 41264002), the 2020 Project of Education Science “13th Five Year Plan” of Gansu Province (GS[2020]GHB4817), and the Education Research Project of Postgraduate Supervisor of Tianshui Normal University (TYXM2307).

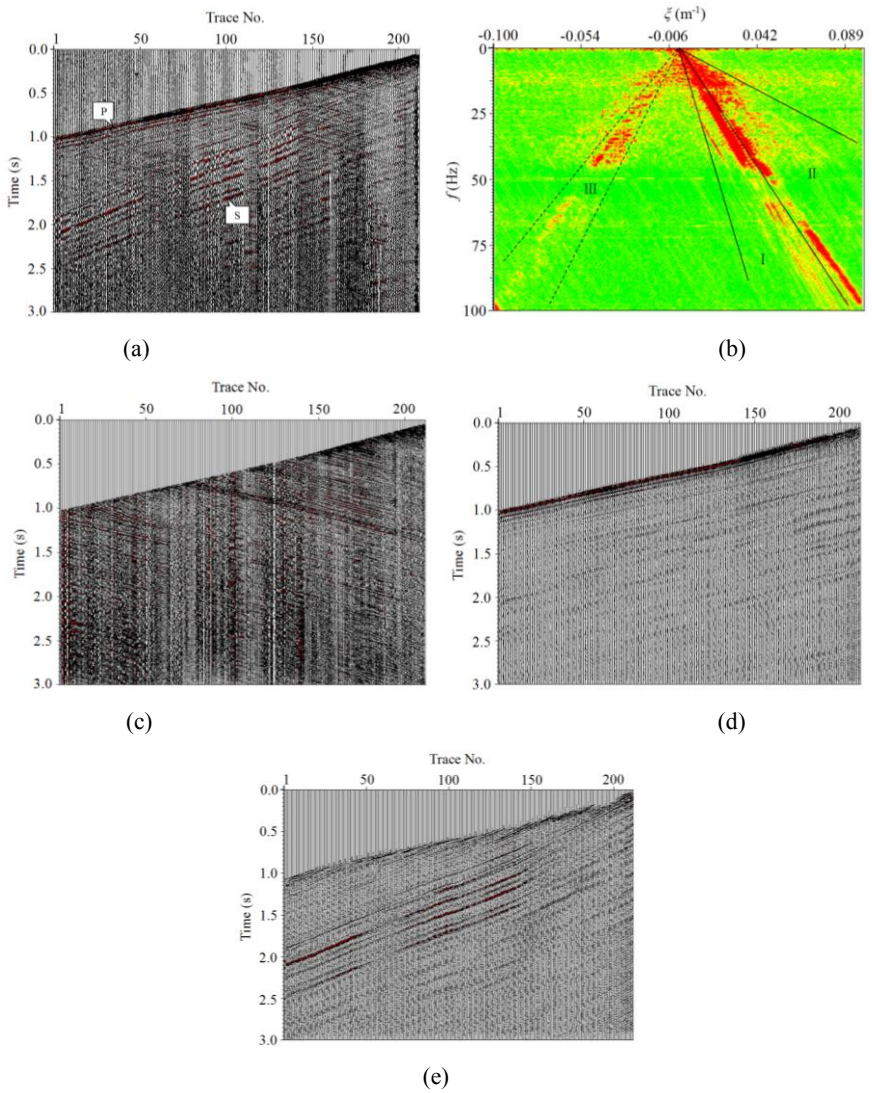

Fig. 4. (a) Real VSP seismogram. (b) f–ξ spectrum of real VSP data. (c) Upgoing waves after removing the downgoing waves by using the presented method. (d) Separated direct P waves. (e) Separated S waves.

References

1. N. de Freslon, L. Cuilhe, S. Yareshchenko, First Break **39**, 35 (2021)
2. W. Moon, A. Carswell, R. Tang, C. Dilliston, Geophysics **51**, 940 (1986)
3. W. Geng, X. Chen, J. Li, J. Ma, W. Tang, F. Wu, Geophysics **87**, V545 (2022)
4. W. sun, Z. Li, Y. Qu, Geophysics **87**, V481 (2022)
5. B. Abbad, B. Ursin, M.J. Porsani, Geophysics **76**, V11 (2011)
6. B. Liu, G. Li, *Proceedings of 2010 international conference on computational and information sciences* (IEEE Computer Society, Chengdu, 2010)
7. M.D. Sacchi, T.J. Ulrych, Geophysics **60**, 1169 (1995)